



**HAL**  
open science

# Impact of Li, Na and Zn metal cation concentration in EMIM-TFSI ionic liquids on ion clustering, structure and dynamics

Samanvitha Kunigal Vijaya Shankar, Yann Claveau, Tojo Rasoanarivo, Chris Ewels, Jean Le Bideau

► **To cite this version:**

Samanvitha Kunigal Vijaya Shankar, Yann Claveau, Tojo Rasoanarivo, Chris Ewels, Jean Le Bideau. Impact of Li, Na and Zn metal cation concentration in EMIM-TFSI ionic liquids on ion clustering, structure and dynamics. *Physical Chemistry Chemical Physics*, 2024, 26, pp.7049-7059. 10.1039/D3CP06315A . hal-04455542

**HAL Id: hal-04455542**

**<https://hal.science/hal-04455542v1>**

Submitted on 13 Feb 2024

**HAL** is a multi-disciplinary open access archive for the deposit and dissemination of scientific research documents, whether they are published or not. The documents may come from teaching and research institutions in France or abroad, or from public or private research centers.

L'archive ouverte pluridisciplinaire **HAL**, est destinée au dépôt et à la diffusion de documents scientifiques de niveau recherche, publiés ou non, émanant des établissements d'enseignement et de recherche français ou étrangers, des laboratoires publics ou privés.

# Impact of Li, Na and Zn metal cation concentration in EMIM-TFSI ionic liquids on ion clustering, structure and dynamics<sup>†</sup>

Samanvitha Kunigal Vijaya Shankar,<sup>a</sup> Yann Claveau,<sup>\*,a</sup> Tojo Rasoanarivo,<sup>a</sup> Chris Ewels<sup>a</sup> and Jean Le Bideau<sup>a</sup>

**Abstract:** We use molecular dynamics calculations to investigate the behavior of metal cations (Li, Na and Zn) within ionic liquids (ILs), specifically EMIM-TFSI, and their impact on key properties, particularly focusing on ion-ion correlations and their influence on diffusion and conductivity. The study explores the competition between metal cations and EMIM ions for binding to TFSI and analyzes ion pair dynamics, revealing that metal cation-TFSI pairs exhibit significantly longer lifetimes compared to TFSI-EMIM pairs. This competitive interaction and the increased stability of metal cation-TFSI pairs at higher concentrations leads to reduced ion exchange, resulting in decreased diffusion and conductivity. The observations underscore the importance of ion size and charge in determining their behavior regarding IL dynamics. Overall, this work provides valuable insights for designing ILs with customized properties, particularly in the context of optimizing conductivity and addressing energy storage challenges.

## 1 Introduction

Room-temperature ionic liquids (ILs) have emerged as useful electrolytes in the field of electrochemistry, offering safer alternative to traditional solvents.<sup>1-3</sup> ILs have found applications in batteries and supercapacitors due to their low flammability, wide electrochemical window, and low volatility.<sup>4,5</sup> In addition, their viscosity decreases with increasing temperature. This makes them particularly suitable for higher operating temperature ranges, as ILs demonstrate good ionic conductivities under such conditions.<sup>6,7</sup> Within this context, there has been a significant surge of interest in developing metal-ion IL-based batteries as potential strategic replacements for conventional Li-ion batteries electrolytes. The ongoing quest for sustainable alternatives to Li<sup>+</sup> includes notably monovalent ions such as Na<sup>+</sup> and divalent ions such as Zn<sup>2+</sup>.<sup>8-12</sup>

Exploration of ILs as electrolytes relies on understanding their dynamical properties such as diffusivity and conductivity. Previous studies have shown that adding metal cations greatly influences the dynamics of IL ions.<sup>13,14</sup> Those metal cations interact with the anions of the IL and this, in turn, affects the dynamics of the system. In particular, several experimental and simulation studies have consistently shown that the introduction of metal cations to ILs significantly influences their viscosity and, consequently, their conductivity:<sup>15-17</sup> experiments, e.g. by Han *et al.*<sup>18</sup> and Martinelli *et al.*,<sup>19</sup> have demonstrated that the conductivities of various Li based ILs decrease due to a combination of factors including ionic association, viscosity, anion size, and thermal properties; molecular dynamics simulations by Kubisiak *et al.*<sup>20</sup> observed a decrease in IL diffusivity and conductivity upon the introduction of lithium or sodium cations, with the effect varying with metal concentration; Borodin *et al.*<sup>21</sup> further explored the structure and transport of monovalent (Li, Na) and divalent (Mg, Zn) metal cations as a function of temperature in PYR<sub>14</sub>TFSI using both molecular dynamics and quantum mechanics.

While these studies highlight the significant impact of con-

centration, nature (monovalent or divalent), size, and electronic structure of the metal ion on the dynamics of the ions in the system, a comprehensive comparative study examining the distinct effects on IL behaviour with the addition of various metallic ions is lacking. Numerical values from molecular dynamics are force field dependent, and it is important to compare results generated using consistent force fields and parameterisations.

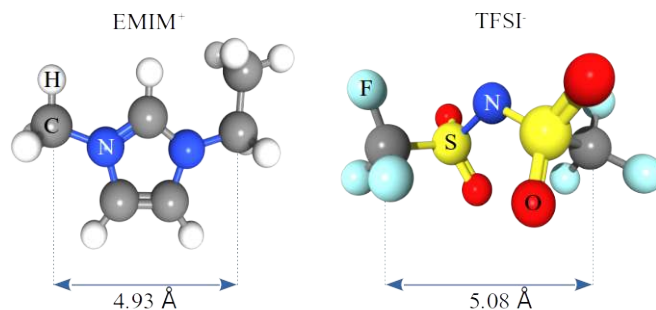


Fig. 1 Ball and stick images for EMIM<sup>+</sup> and TFSI<sup>-</sup> ions. In all our simulations, atoms are free to rotate around bonds. Hence, in case of TFSI, distances between carbons at the end vary (example distance shown correspond to the configuration of TFSI in the figure).

This current study explores dynamic aspects of the interplay between different metal cations, i.e. Li<sup>+</sup>, Na<sup>+</sup> or Zn<sup>2+</sup> and a host IL, ethyl,methylimidazolium (EMIM) and bis(trifluoromethylsulfonyl)imide (TFSI) (Fig. 1). The EMIM-TFSI ionic liquid is chosen as it is well-known and well-studied,<sup>22</sup> with a stable electrochemical potential window up to 4.6 V.<sup>23</sup> It also shows a high conductivity well adapted to supercapacitors operating above room temperature. The addition of metal salt is desirable for pseudosupercapacitors and hybrid systems, in order to provide higher power and higher energy density systems.<sup>24</sup> Using classical molecular dynamics simulations, our aim is to understand the interactions between the different species through a thorough comparison of structural and dynamic properties as a function of concentration, temperature and metal cation type.

<sup>a</sup> Nantes Université, CNRS, Institut des Matériaux de Nantes Jean Rouxel, IMN, F-44000 Nantes, France

\* E-mail: yann.claveau@cnrs-imm.fr

<sup>†</sup> Electronic Supplementary Information (ESI) available

## 2 Computational method

Simulations were conducted using the LAMMPS molecular dynamics package.<sup>25</sup> Input files were prepared with the help of fftool<sup>26</sup> and packmol.<sup>27</sup> Resultant atom trajectories were analysed using the TRAVIS package,<sup>28</sup> MDAnalysis,<sup>29,30</sup> and in-house Python scripts.

We first studied neat EMIM-TFSI as a reference, before mixing EMIM-TFSI with varying concentrations of monovalent (Li(TFSI), Na(TFSI)) and divalent (Zn(TFSI)<sub>2</sub>) salts. The non-polarisable CL&P force field<sup>31</sup> was used for EMIM<sup>+</sup>, TFSI<sup>-</sup>, Li<sup>+</sup>, and Na<sup>+</sup>. For Zn<sup>2+</sup>, which is not currently included in CL&P, we used Stote parameters,<sup>32</sup> which are also based on standard 12-6 Lennard-Jones and Coulomb potentials.

An infinite liquid is simulated using a periodic box. We ensured that the cubic box is large enough to avoid finite size effects (typically a width  $w$  at least four times the van der Waals radius cut-off, *i.e.*  $w \sim 50 \text{ \AA}$ ), through a convergence study of diffusion coefficient in NVT simulations on EMIM-TFSI, from  $w = 40$  to  $60 \text{ \AA}$ . As a result, our neat EMIM-TFSI system contains 300 ion pairs contained in a cubic box with side length  $51.47 \text{ \AA}$ . The concentration of the added salt was varied from  $n_{\text{Me}^+}/n_{\text{Me}^+ + \text{EMIM}^+} = 0.04$  to 0.24 cationic molar fraction. The resultant compositions of all the systems are detailed in Table 1.

Table 1 Composition of the simulated systems for metal cations Li, Na and Zn. Cationic molar fractions are given in parentheses

Nb of Metal cations (concentration)	Nb of EMIM cations (concentration)	Nb of TFSI anions	
		with Li/Na	with Zn
12 (0.04)	288 (0.96)	300	312
36 (0.12)	264 (0.88)	300	336
72 (0.24)	228 (0.76)	300	372

A time-step of 1 fs was used throughout, with atomic coordinates stored every 2 ps. Long range electrostatic interactions were solved using the PPPM solver. The cutoff for long range interactions was set at  $12 \text{ \AA}$ . The Shake algorithm was used to constrain H bonds. The systems were equilibrated in the NPT ensemble at  $P = 1 \text{ atm}$  for 10 ns until the density was fully converged. The systems were then further equilibrated in the NVT ensemble for 10 ns. Production runs were carried out in the NVT ensemble for 50 to 70 ns depending on the temperature. All runs at 393 K were carried out for 50 ns except the ion-pair lifetimes for the Zn system which ran for 180 ns, due to the long stability lifetimes of Zn-TFSI pairs. In principle one should avoid using NVT for production runs since thermostats can affect the dynamics of the system. However, NVT simulations are computationally less expensive and more stable than NVE simulations. To ensure that the NVT ensemble is an acceptable approximation, we verified that the use of a Nose-Hoover thermostat does not affect significantly the dynamics of our systems (more details in ESI).

Representative convergence studies are given in ESI, including densities that are in good agreement with experiment (less than 2% deviation where experimental data available).

## 3 Results and Discussion

### 3.1 Analysis of Self Diffusion Coefficients

The average self diffusion coefficients of all the ions in the system are obtained through the Einstein relation from mean squared displacement (MSD) calculations:<sup>33</sup>

$$D = \frac{1}{2d} \lim_{t \rightarrow \infty} \frac{d}{dt} \left\langle \frac{1}{N} \sum_{i=1}^N |\vec{r}_i(t) - \vec{r}_i(t_0)|^2 \right\rangle_{t_0} \quad (1)$$

where  $d$  is the dimensionality of the system,  $N$  is the number of ions,  $\vec{r}_i(t)$  is the position of ion  $i$  at time  $t$ , and  $\langle \cdot \rangle_{t_0}$  denotes an average over all starting times  $t_0$ .

The calculated values for the Li<sup>+</sup> system are shown in Figure 2. In general the EMIM self-diffusion coefficients are approximately twice that of the TFSI, which are themselves roughly twice that of the Li. The diffusion coefficients of all the ions in the system increase continuously with temperature, as expected. This allows us to focus on the system at high temperature, *i.e.* 393 K, to ensure faster dynamics and reduce the computational cost. The self diffusion coefficients in the Na<sup>+</sup> and Zn<sup>2+</sup> systems as a function of temperature behave very similarly, and are given in ESI.

We next explore the variation in self-diffusion coefficient as a function of metal cation concentration at 393K. Figure 3 shows that while, in general, all the ion self-diffusion coefficients decrease with increasing metal cation concentration, there are some ion-specific features. This is in good agreement with previous simulations performed with different parameters for Na and Li.<sup>34,35</sup> We note that these self-diffusion coefficients are around one order of magnitude lower than those reported in experiments,<sup>36</sup> a discrepancy commonly seen in studies of ILs when using non-polarisable force fields. However, it has been shown that this does not impede the analysis of relative trends.<sup>37</sup>

As the concentration of metal cations increases, the diffusion

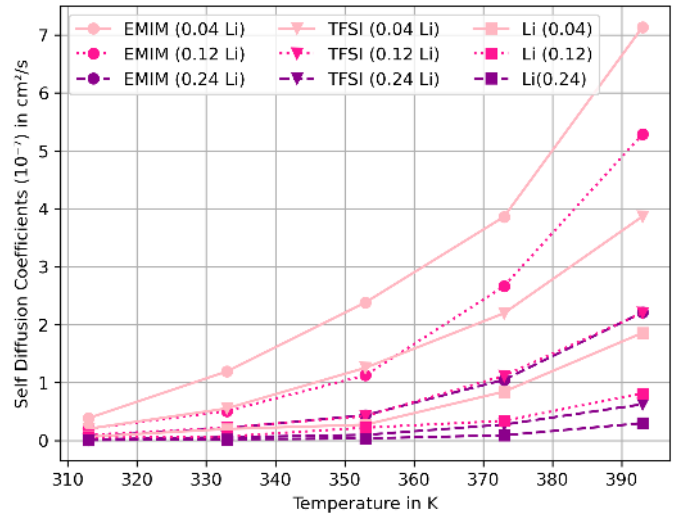


Fig. 2 Calculated self-diffusion coefficients ( $10^{-7} \text{ cm}^2\text{s}^{-1}$ ) of the component ions in bulk Li-EMIM-TFSI, as a function of temperature (K), with Li concentrations of 0.04 (rose), 0.12 (pink), and 0.24 (magenta). Symbols represent EMIM (circles), TFSI (triangles) and Li (squares).

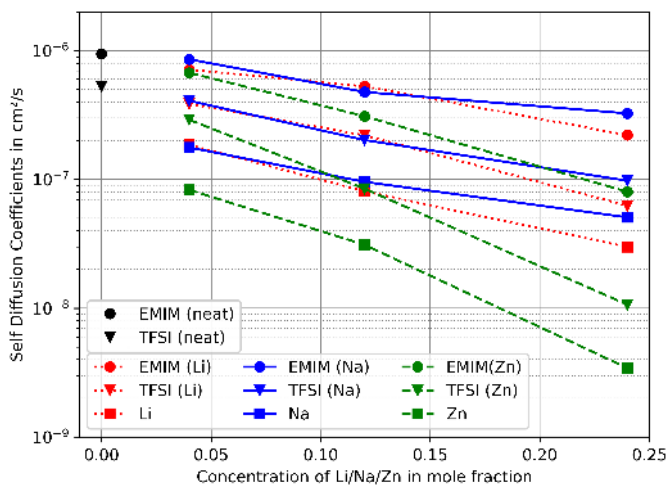


Fig. 3 Calculated ion self-diffusion coefficients in  $\text{Me}_x\text{-EMIM}_{1-x}\text{-TFSI}$  systems ( $\text{Me}=\text{Li}, \text{Na}, \text{Zn}$ ), as a function of concentration  $x$  at  $T = 393 \text{ K}$ . Red dotted lines indicate Li based IL, blue lines are for Na and green dashed lines for Zn. Circles show EMIM cations, triangles for TFSI anions and squares for metal cations.

coefficients of both TFSI and metal cations decrease. This is consistent with an increasing number of TFSI anions bound to the metal cations as the metal concentration increases and is discussed further in Section 3.3.

Turning to the metal cations, both Na and Li show very similar self-diffusion coefficients (although  $D_{\text{Na}}$  decreases slower than  $D_{\text{Li}}$  with concentration), significantly larger than that of Zn. This suggests that ion charge state is a key driver in determining self-diffusion. This is despite the possibility of  $\text{Na}^+$  ions potentially being able to pair with more TFSI due to their size (see Section 3.2 below). In contrast, the divalent cation  $\text{Zn}^{2+}$ , due to its double valency and size comparable to  $\text{Li}^+$ , is expected to interact more strongly with the TFSI ions in the system, resulting in the lowest diffusion coefficients.

Interestingly, we also note a reduction in the self-diffusion coefficients of the EMIM ions concurrent with an increase in metal cation concentration, even though we do not expect them to be directly coupled. However, analysis of the underlying mechanisms resulting in these trends in diffusion coefficient, in particular for  $D_{\text{EMIM}}$ , is difficult based only on system averaged data. In order to obtain more insight into the processes at play, it is necessary to examine the local structure, as well as the diffusive behaviour of individual ions within the overall population.

### 3.2 Structure Analysis

The diffusion process is intimately tied to the structure. Therefore, a thorough understanding of the structure will help in comprehending the interactions among the different species. For this reason, radial distribution functions (RDF) are plotted as a function of concentration and nature of metal cation. Figures 4a and 4c show the RDF of TFSI oxygen atoms ( $\text{O}_{\text{TFSI}}$ ) and centers of mass of TFSI ions themselves around the metal cations. Figures 4b and 4d show the corresponding integrated RDFs, which represent the associated coordination numbers for oxygen atoms

and TFSI centers of mass around metal cations respectively.

Interestingly the local structure seems to be largely independent of the metal cation concentration. The first solvation shells of  $\text{O}_{\text{TFSI}}$  around  $\text{Zn}^{2+}$  and  $\text{Li}^+$  are both situated at  $2.1 \text{ \AA}$ , whilst for  $\text{Na}^+$  it is further away at  $2.5 \text{ \AA}$  (Fig. 4a). This largely reflects their respective ionic radii:  $\text{Zn}^{2+}$  ( $0.88 \text{ \AA}$ ) and  $\text{Li}^+$  ( $0.90 \text{ \AA}$ ), being smaller than  $\text{Na}^+$  ( $1.16 \text{ \AA}$ ), can be in closer proximity to the oxygen atoms. In each case there is a single O-cation distance, with a sharp peak for Zn, slight broadening for Li, and significant broadening for Na. This broadening reflects the binding strength to the ion (the ion's "softness"), again primarily due to the cation charge state and the distance of the oxygen from the cation nucleus. A broader secondary peak around  $2.2 \text{ \AA}$  further from the cation represents the oxygen atoms attached to the second sulphur of TFSI. The integrated RDF for  $\text{O}_{\text{TFSI}}$  (Fig. 4b) around  $\text{Me}^+$  shows clearly six oxygen atoms around Zn, corresponding to an octahedral configuration (Fig 5). The Na and Li form a much less pronounced plateau, converging to between five and six oxygen neighbours, suggesting similar oxygen octahedral coordination but with significantly more structural variation.

Unlike the single peak for individual  $\text{O}_{\text{TFSI}}$ , the distribution of TFSI molecules around Li and Na show two distinct peaks, again with the TFSI slightly further from the Na (Fig. 4c). From the integrated RDF (Fig. 4d) the closer peak corresponds to around 2 TFSI molecules for Li and Na, with 2 further TFSI molecules described by the second peak. Since 5-6 oxygens sit around the Li and Na, together these results suggest that Li and Na have, on average, two more tightly bound TFSI and two slightly further away, and of these, typically two are bound via a single oxygen atom and two with two oxygens. Previous experimental results obtained by decomposition of Raman spectra show a signature associating 2 TFSI per  $\text{Li}^+$ ,<sup>38</sup> suggesting the more weakly bound pair seen in the RDF are not detectable in Raman.

The Zn-TFSI RDF is more complex since the second peak also has a slight shoulder at about  $4.2 \text{ \AA}$ . The integrated RDF (Fig. 4d) shows that there are on average 0.5 - 0.8 TFSI most closely bound to Zn, and around 5.5 - 5.2 TFSI in total when all three peaks are integrated. These fractional values can either come from an average over different configurations, or could be linked to time averaging of the RDF over the whole production run (see Section 3.4). Considering the 0.24 molar cation concentrations where the total TFSI in the coordination shell converges cleanly to 5.2, these results suggest that in the majority of cases, TFSI are arranging in a distorted octahedron around the Zn. The integrated RDF shows that there is one closer TFSI site, one intermediate and four slightly further away, however the closer TFSI site is not always occupied. Given the oxygen coordination is stable at six, this suggests that in the cases where the closer TFSI is not occupied, one of the other TFSI has two oxygen atoms bound to Zn, likely associated with the observed peak shoulder in the Zn-TFSI RDF. These configurations are represented by two snapshots in Fig. 5 where the octahedron cages of 6 oxygens is made by 6 or 5 TFSI.

Similar results have been obtained regarding the coordination of oxygen of TFSI in  $\text{PYR14-TFSI}$  with metal cations.<sup>21</sup> However, they found that most of  $\text{Zn}^{2+}$  solvates was dominated by bidentate coordination configurations (3 TFSI sharing 2 oxygens).

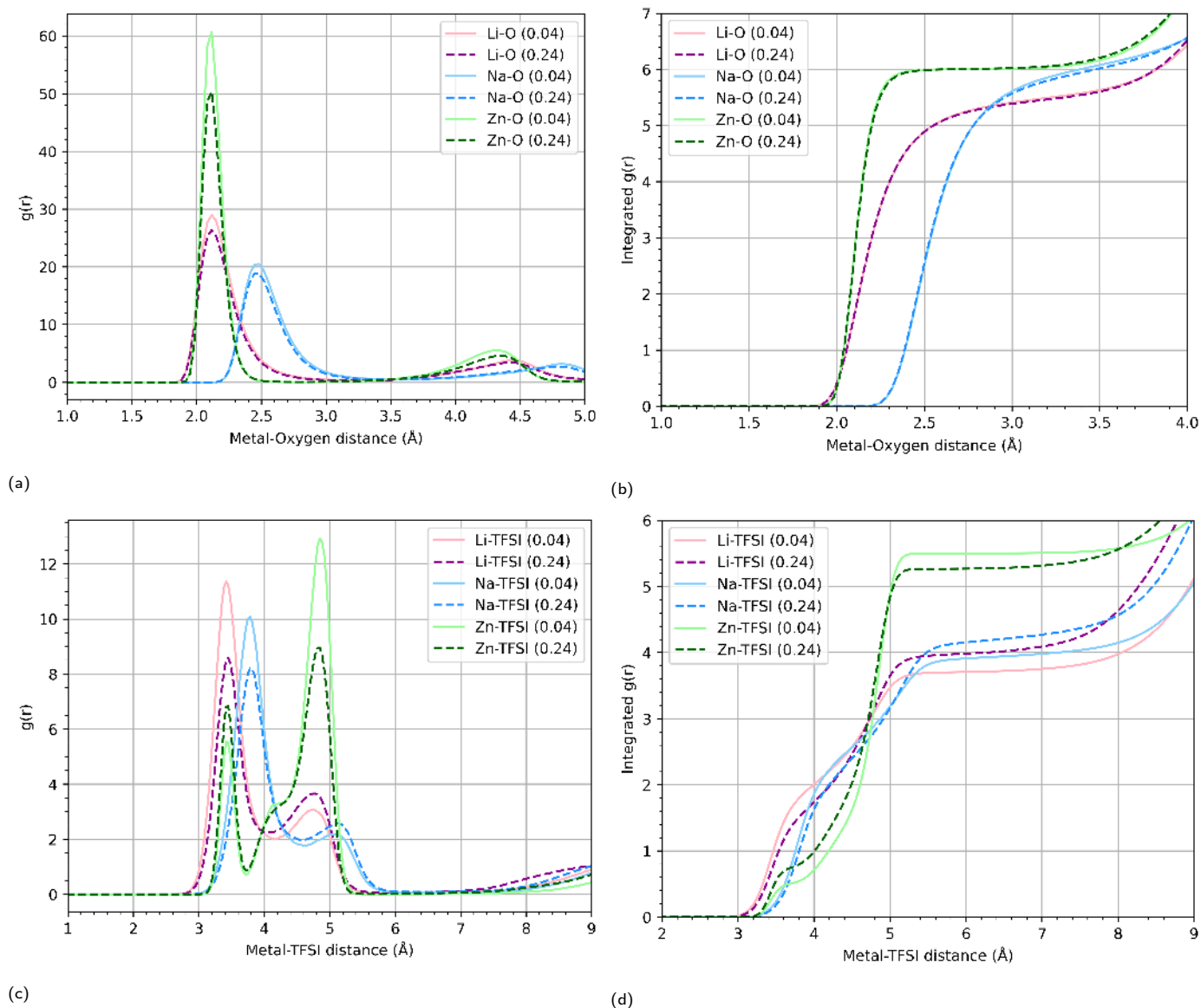


Fig. 4 Radial distribution functions for (a) TFSI oxygen atoms and (c) TFSI ions, around metal cations (Li, Na and Zn). Coordination number of (b) TFSI oxygen atoms and (d) TFSI ions around metal cations. Magenta indicates Li systems, blue for Na and green for Zn. Light colors (solid lines) are for low metal cation concentration (0.04), dark colors (dashed lines) for high concentration (0.24). System temperature is 393 K, all distances in Å.

These differences could be due to the different cation of the IL (PYR14 instead of EMIM) or more likely to the use of a polarisable force field. Indeed, another study on EMIM-TFSI<sup>20</sup> showed that the use of non-polarisable force field tend to increase the fraction of monodentate interactions between the Li or Na cation and TFSI anions, which in turn decreases the diffusivity. However, they have also showed that the non polarisable force field better reproduce experimental trends than Drude-particle force field, although the latter performs better quantitative estimates of diffusion coefficients and conductivities.

We note that at the highest 0.24 cation molar concentration, if each of the 72 Zn was surrounded by 5.2 unique TFSI molecules this would require 374 TFSI molecules, that is to say all the TFSI (see Tab. 1). This implies that either some TFSI molecules must be shared between Zn atoms, or that the system no longer has

any TFSI interacting only with EMIM. The same conclusion can be drawn for cations in the other systems, for example in 0.24 Li and Na, if each cation had 4 unique TFSI neighbours, that would require 288 of the 300 TFSI molecules in the system.

The above structural analysis is consistent with the observed diffusivity (Fig. 3), where  $\text{Zn}^{2+}$  diffuse slower due its stronger interaction and its greater number of tightly bound TFSI, and although  $\text{Na}^+$  ions have more oxygen around them than  $\text{Li}^+$ , their soft interaction (broad peak, "soft" solvation shell) allows them to diffuse faster than  $\text{Li}^+$ . However, while the structural analysis can explain the varying diffusion speeds of the metal cations, it does not provide an explanation for the observed decrease in EMIM cation diffusion with increasing metal-cation concentration. To address this, dimer lifetime analysis is required.

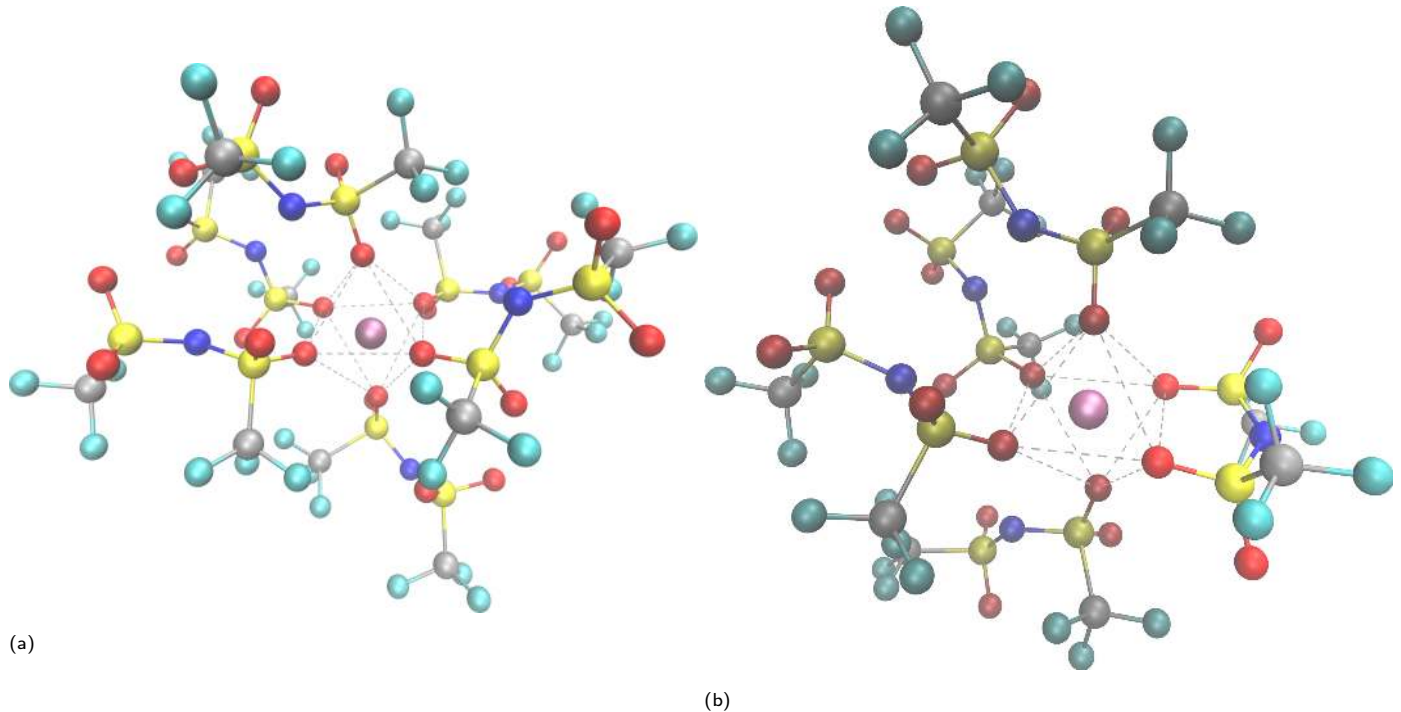


Fig. 5 Snapshots of (a) 6 TFSI in octahedral configuration around  $Zn^{2+}$  and (b) 5 TFSI in octahedral configuration around  $Zn^{2+}$  with one of the TFSI sharing 2 oxygens with TFSI.

### 3.3 Lifetime Analysis of Ion Pairs

The dynamics of ILs is predominantly governed by ion-ion correlations, which can be described via correlation functions between different ion types. Here, we use dimer existence auto correlation functions (DACF) as implemented in TRAVIS.<sup>28</sup>

A DACF for a given set of particles is defined as a function that retains a value of 1 as long as the specified criteria are met, and transitions to 0 once the criteria are no longer satisfied, i.e.

$$c(\tau) = \frac{1}{N^2} \sum_{i=1}^N \sum_{j=1}^N \int_0^\infty \beta_{ij}(t) \beta_{ij}(t + \tau) dt \quad (2)$$

where,  $\beta_{ij} = \begin{cases} 1 & \text{if criteria is satisfied} \\ 0 & \text{otherwise} \end{cases}$ . In this study, threshold

distance criteria have been chosen as follows. For EMIM-TFSI pairs, they are considered to be paired if the distance between the geometric centre of the two species is less than the sum of the maximal molecular radii  $r_{EMIM} + r_{TFSI} = 7.80 \text{ \AA}$ . The cut-off distances for metal cation-TFSI are chosen from the end of the first solvation peak in the cation- $O_{TFSI}$  RDF (Fig. 4a), and set to  $3.35 \text{ \AA}$  for Li-TFSI,  $3.56 \text{ \AA}$  for Na-TFSI and  $2.80 \text{ \AA}$  for Zn-TFSI.

Using the above criteria, the lifetime  $T$  of the aggregate is then twice the total integral of this auto-correlation function  $c(\tau)$ :

$$T = 2 \int_0^\infty c(\tau) d\tau \quad (3)$$

Figure 6 shows the lifetime of different TFSI-cation complexes as a function of metal cation concentration. The metal cation-TFSI species have lifetimes one to two orders of magnitude longer than TFSI-EMIM, consistent with their stronger binding. The

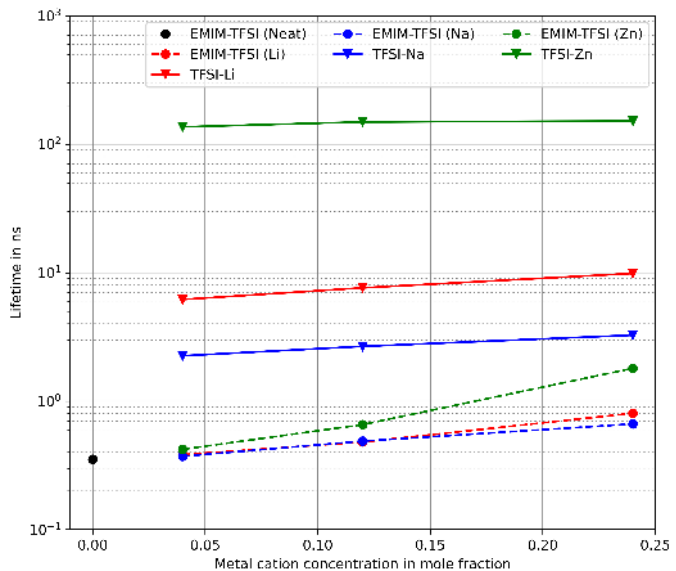


Fig. 6 Lifetime of different ion pairs in the system as a function of metal ion concentration (Eq. 3), at 393K. Circles are for EMIM-TFSI pairs, triangles for TFSI-metal ones. Black represents neat IL, red is for Li based ILs, blue for Na based ones and green for Zn based ion pairs.

lifetime ordering for metal cation-TFSI is in agreement with the structural data in Section 3.2 and the calculated ion self-diffusion coefficients (Fig. 2). The shortest lived species are Na-TFSI with average lifetime from 2.3-3.3 ns, while Li-TFSI is around three times longer (around 9ns). This explains why, despite having more oxygen in its first solvation shell,  $\text{Na}^+$  maintains a diffusion coefficient similar to that of  $\text{Li}^+$  (Fig. 3) due to this higher exchange rate of TFSI ions. Zn-TFSI lifetimes are over 50 times longer than Na (around 120 ns), consistent with the calculated strong Zn-TFSI binding, and its low self-diffusion coefficient. During the calculation runs of 50 ns for Na and Li, there is therefore extensive breaking and reforming of cation-TFSI pairing (notably for Na), whereas for Zn-TFSI the complexes are extremely stable, even over the extended 180 ns calculation period chosen.

As the concentration of metal cation increases, the interaction between the metal cation and TFSI becomes more pronounced and persists for a longer duration, partly also because there is then less "free" TFSI available for exchange. This is manifested by the extended lifetime of metal cation-TFSI dimers at higher concentrations, in turn resulting in slower diffusion of the metal cations. These longer metal cation-TFSI interactions clearly dominate the briefer EMIM-TFSI encounters, thereby influence the dynamics of the entire system. This can be seen by the increase in EMIM-TFSI lifetime with increasing metal cation concentration, and explains the decrease in diffusion rate of EMIM and TFSI ions in metal cation-EMIM TFSI system in comparison to neat EMIM-TFSI (Fig. 3). Since these are the majority carriers in the system, this is also linked to experimentally observed viscosity increases. The lifetime increase is most evident in Li-TFSI (increase of 60% going from 0.04 to 0.24 molar concentration), compared to 45% for Na and only 11% for Zn.

Considering the lifetime data as a whole we can start to build an overall picture of ion behaviour in these systems. At lower metal cation concentration, TFSI-Na and TFSI-Li clusters are shorter lived, with the metal cations more mobile consistently. The remaining TFSI-EMIM form short-lived, relatively weakly bound couples. As the metal cation concentration increases, there is an increased trend to forming more stable, longer-lived TFSI-metal clusters, which slow the metal cations down. This also structures and "rigidifies" TFSI-EMIM exchange with less overall TFSI mobility, leading to a slight increase in lifetime of TFSI-EMIM clusters as a result. Within this picture there are differences for the different metal cations.  $\text{Na}^+$  is larger and less tightly bound to TFSI, hence maintaining shorter lived clusters and a higher diffusivity as a result. In stark contrast  $\text{Zn}^{2+}$  is tightly bound to its TFSI neighbours, forming extremely long-lived clusters with a very low metal cation diffusivity.

### 3.4 Distribution of diffusion coefficients

The above analysis is primarily focused on trends exhibited by averaged observables. While this approach provides a broad overview of the behaviour, it may mask discrete behaviours within the ILs. By plotting the distribution of these quantities, it is possible to reveal the existence of multiple distinct populations.

To achieve this, the entire MSD curve for each individual ion in

the system was fitted. Even though such a fit does not represent the diffusive regime as per standard MSD curves ( $\lim_{t \rightarrow \infty} \frac{d\text{MSD}}{dt}$ ), it still yields a value (the slope) that we can term as the "overall diffusion coefficient" for that ion. This value accounts for the entire path traversed by the given ion throughout the simulation run, thereby eliminating the occurrence of negative diffusion coefficients due to poor fits for some ions. To enhance statistical robustness, nine sets of different trajectories have been accumulated.

The distribution of diffusion coefficients of EMIM, TFSI and metal ions are plotted for two molar ratios of metal cations (0.04 and 0.24) in Fig. 7. In general the metal cations show the smallest full width half maximum (FWHM) in the diffusion coefficient values, indicating they show relatively uniform behaviour. The distribution in TFSI values is roughly twice that of the metal ions. EMIM shows the highest range in values, with FWHM 3-4 times that of the TFSI, more consistent with conventional liquid behaviour. In all cases the distribution appears monomodal, although we cannot exclude the possibility of two peaks that are partially overlapping due to the use of window algorithm. This algorithm increases the statistics by iterating over the reference time. However, this approach could potentially mask a bimodal distribution. The reason is that the window algorithm averages over different time windows, which could blend two distinct peaks into a single one if these peaks occur in different time windows. Therefore, while the window algorithm enhances the overall statistics, it might also mask the presence of multiple distinct behaviors in the diffusion coefficients. Even when we analyze the mean square displacement (MSD) of each ion separately, this sum over  $t_0$  could still potentially hide a bimodal distribution. Hence, while our results suggest a monomodal distribution, further analysis with a different method might be necessary to confirm this.

The most notable change occurs with increased metal cation concentration, which greatly decreases the spread in distribution of diffusion coefficients, as well as decreasing the fitted maximum. Notably this behaviour is also seen in the EMIM population, as well as the TFSI and metal cations. This clearly shows that increasing the metal cation concentration renders the whole system more homogenous, reducing the spread of faster diffusing ions. This suggests the metal cations are reducing variability in the system, rendering it more ordered and "rigid". This is consistent with the calculated increase in ion-pair lifetimes seen above.

Comparing the metal cations, the distribution width of metal cation diffusion coefficients for Li, Na and Zn reflect the strength of the metal-cation binding. At 0.24 molar concentration the broadest distribution in cation diffusion coefficients is for Na (FWHM of  $7 \times 10^8 \text{ cm}^2/\text{s}$ ), with Li approximately half this, and Zn nearly 20 times smaller. This is fully consistent with the RDF data and local structure discussion presented above.

Building on the analysis of diffusion coefficients and dimer lifetimes, we have shown that the lifetime of metal-TFSI pairs significantly influences the overall diffusion. Increasing the quantity of metal-TFSI pairs orders the whole system, reducing the amount of TFSI available to pair to EMIM, and it is these more weakly interacting species that are dominating the system diffusion. The

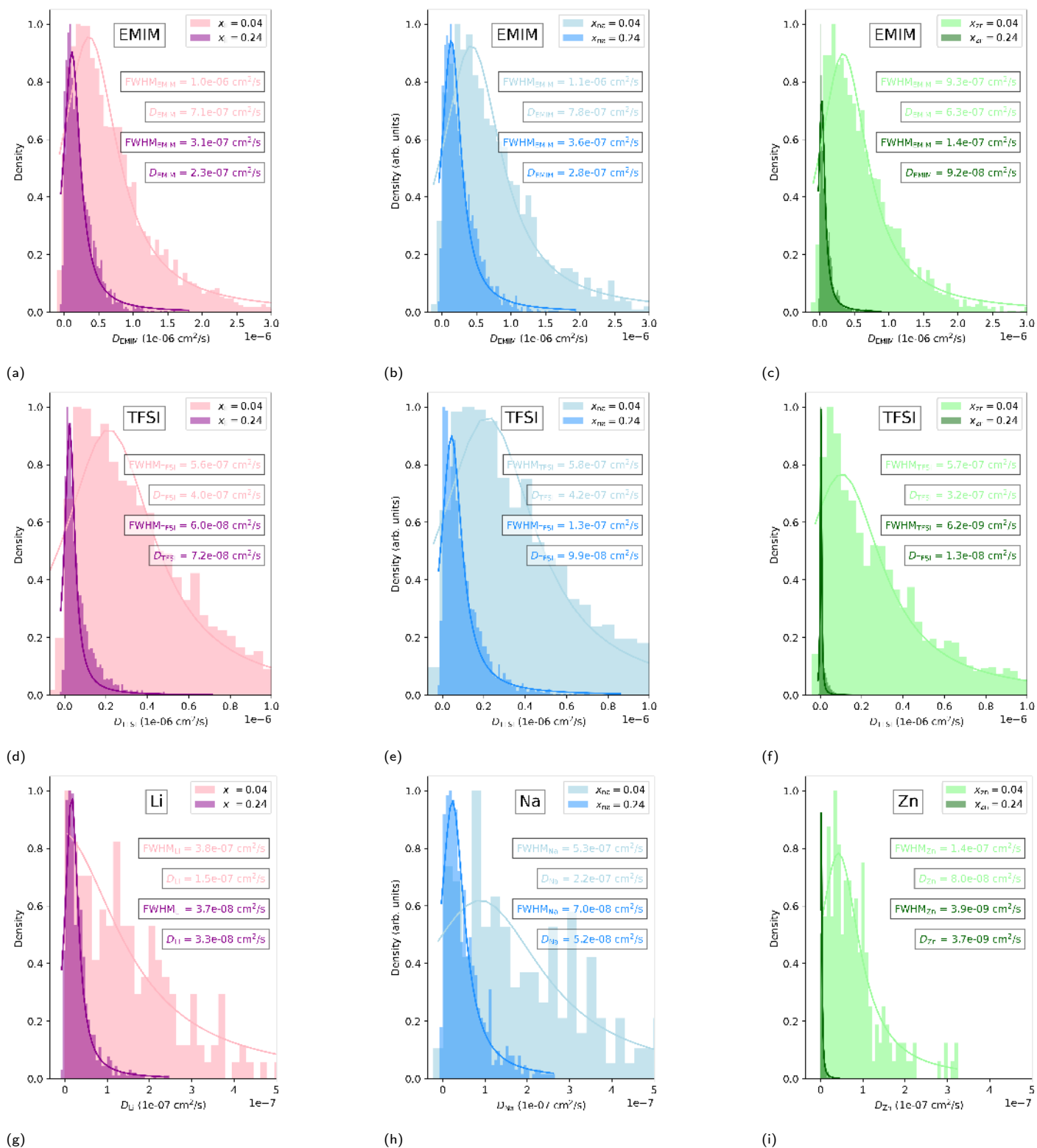


Fig. 7 Histograms of diffusion coefficients of individual ions in the system as a function of metal cation molar concentration. Pink, blue and green are Li, Na and Zn based ILs respectively. First, second and third rows show distribution of diffusion coefficient of EMIM, TFSI and metal cations respectively. Densities have been normalized by their maximum to make reading easier. Full width half maximum (FWHM) and average density coefficients are indicated each plot based on a Gaussian fit.

effect of adding more metal cations on EMIM diffusivity therefore suggests that the primary impact of metal cations on overall conductivity is indirect rather than direct. To explore this in more detail, we next turn to conductivity calculations.

### 3.5 Conductivity

Conductivity of a system is the collective dynamic property obtained due to the contribution of all the interactions between different pairs of ions in the system. It is derived from ion-ion correlation function while accounting for the charge of the interacting species.

The ionic conductivity of the systems is derived from the Green-Kubo relation and reads as follows:

$$\sigma = \frac{1}{6k_B T V} \lim_{t \rightarrow \infty} \frac{d}{dt} \left\langle \sum_{i=1}^N \sum_{j=1}^N q_i q_j [\vec{r}_i(t) - \vec{r}_i(t_0)] \cdot [\vec{r}_j(t) - \vec{r}_j(t_0)] \right\rangle \quad (4)$$

Where  $t_0$  refers to initial time,  $q_i, q_j$ ,  $\vec{r}_i, \vec{r}_j$  refer to the charge and position of the  $i^{th}$  and  $j^{th}$  particles and  $\langle \cdot \rangle$  denotes the ensemble average of the system.

Correlation between particles implies that their movements are not independent; the displacement of one particle is associated with the displacement of another. In Eq. 4, the dot product of the displacement vectors of the  $i$ -th and  $j$ -th particles,  $[\vec{r}_i(t) - \vec{r}_i(t_0)] \cdot [\vec{r}_j(t) - \vec{r}_j(t_0)]$ , quantifies this correlation. A positive dot product indicates that the particles move in the same direction, while a negative dot product means movement in opposite directions. This leads to four possible scenarios:

- When  $q_i$  and  $q_j$  have the same sign ( $q_i q_j > 0$ ):
  - If the particles are correlated and move in the same direction (forming a charged aggregate), their contribution to the conductivity is positive.
  - If they move in opposite directions, their contribution is negative.
- When  $q_i$  and  $q_j$  have opposite signs ( $q_i q_j < 0$ ):
  - If the particles are correlated and move in the same direction (forming a neutral aggregate), their contribution to the conductivity is negative.
  - If they move in opposite directions, their contribution is positive.

The formula for ionic conductivity derived from the Green-Kubo relations, as shown in Eq. 4, offers several advantages over the Nernst-Einstein equation  $\sigma = \frac{N_{ions}}{V k_B T} \sum_{i=1}^{N_{species}} q_i^2 D_i$ . Firstly, it takes into account the correlations between the movements of different ions, which the Nernst-Einstein equation does not (although other groups have successfully proposed ways to exploit the Nernst-Einstein equation<sup>39</sup>). This makes it a more accurate representation of the actual behavior of ions in a real system, where the movements of ions are often correlated due to their strong electrostatic interactions with each other. Secondly, the Green-Kubo formula for ionic conductivity is directly related to values that can be measured with dielectric spectroscopy. Dielectric spectroscopy

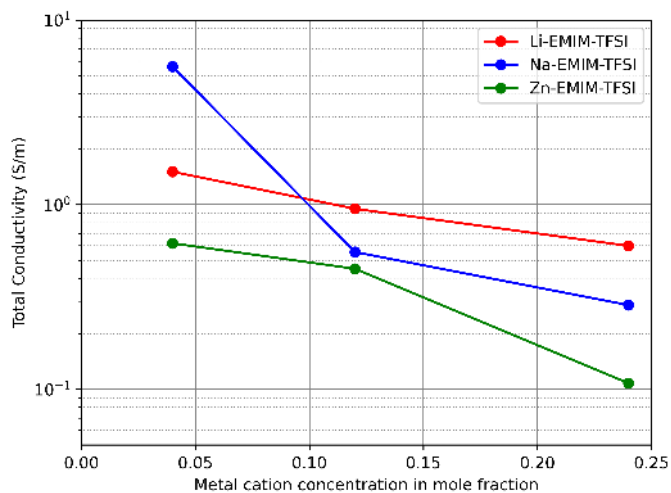


Fig. 8 Total conductivity using Green-kubo formula in function of metal concentration.

measures the response of a material to an applied electric field, which is directly related to the movements of charged particles within the material. Therefore, the Green-Kubo formula provides a theoretical basis for understanding the results of dielectric spectroscopy measurements.

Using the above formula, the conductivity of the different systems is represented in Fig. 8. It shows that the conductivity decreases with increase in concentration of metal cation like diffusivities and dimer lifetimes.

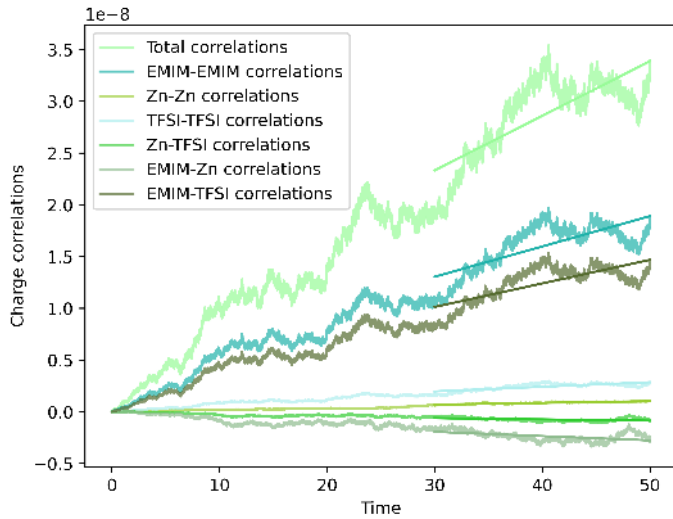
Although Zn systems possess the lowest diffusion coefficients, relatively more TFSI around  $Zn^{2+}$ , longest lifetime for Zn-TFSI ion pairs due to the divalency of  $Zn^{2+}$  ions and their small sizes, the ionic conductivities of the three systems remain quite close, similar to EMIM-TFSI dimer lifetimes.

Similarly to Ref.<sup>20</sup> we have calculated the different correlations in Eq. 4: Me-TFSI, Me-EMIM, EMIM-TFSI, EMIM-EMIM, TFSI-TFSI, Me-Me. Figure 9 represents these contributions for a Zn concentration of 0.04. Others systems can be found in ESI.

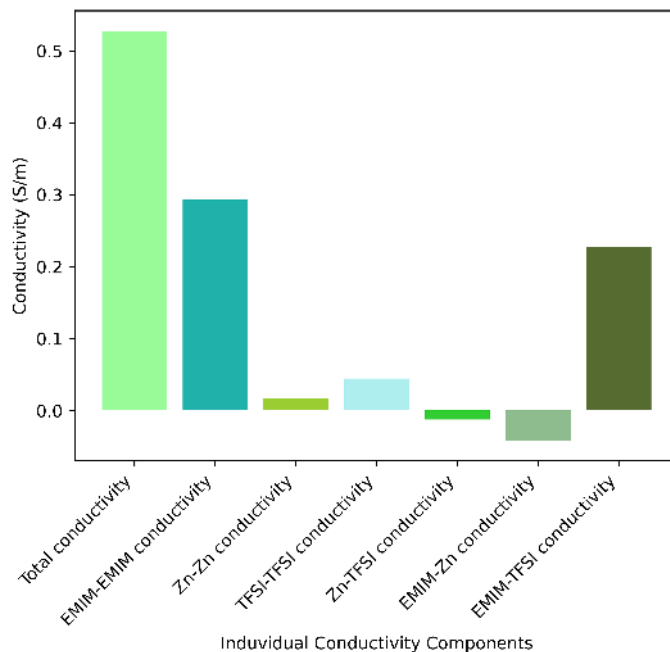
Firstly, it is important to acknowledge the substantial uncertainty surrounding the conductivities. The conductivity can fluctuate significantly (ranging from half to double), particularly at lower metal concentrations, depending on the time range over which the charge correlations have been fitted. This aligns with the diffusion coefficient histograms (Fig. 7), which also have a wider distribution at lower metal concentrations. We see the same pattern here: at lower concentrations, charge correlations vary greatly from one pair to another, resulting in these erratic curves. Therefore, it's risky to compare different systems.

However, one commonality is that the primary contributors to conductivity are, firstly, EMIM-EMIM pairs and, secondly, EMIM-TFSI pairs. For the same reason, despite the Zn-TFSI dimer having a very long lifetime, 50 ns runs are adequate for analyzing correlations since metal-ion pairs don't significantly contribute to conductivity.

This observation is consistent with the observed dimer lifetime: metal-cations are stuck to TFSI while EMIM cations can



(a)



(b)

Fig. 9 (a) Correlations between ion pairs and (b) their corresponding conductivity, for Zn-EMIM-TFSI with a Zn concentration of 0.04. 15 trajectories have been used at 0.04, for 50 ns and 9 for others concentrations. The conductivity is proportional to the slope of the correlation at large time.

exchange their counterions. However, by increasing the concentration, EMIM becomes more strongly paired to TFSI. To increase the conductivity it is then crucial to decrease correlations between the metal ion and its counterion.

Due to the poor statistics it is impossible to discuss the correlation trends in greater detail. The use of a window algorithm (iterating over initial time to artificially increase the number of trajectories) or additional trajectories should be considered. However, the use of window algorithm, as in the case of the diffusion coefficient distribution, could potentially mask certain features of the data. Specifically, if there are multiple distinct correlation trends present, the window algorithm could blend these into a single trend due to its averaging over different time windows. This could result in the loss of information about individual trends and make it appear as though there is only a single, uniform correlation trend. Therefore, while the window algorithm can enhance the overall statistics and allow for a broader analysis, it may also obscure the presence of multiple distinct behaviors in the correlation trends. Consequently, while it is a useful tool, its use should be complemented with other methods to ensure a comprehensive analysis.

## 4 Conclusions

The study shows that all dynamical properties exhibit a decrease with increasing concentration of metal-cations. A notable competition is observed between metal-cation and EMIM in their propensity to form a bond with TFSI. At high concentration, the metal cation-TFSI ion pairs are more stable and persist for a longer duration, which in turn leads to a decrease in the number of free TFSI ions. This results in a decrease in TFSI ions to

interact with EMIM ions, which in turn leads to a decrease in the number of "free" EMIM ions, hence to diffusivity and conductivity.

The diffusion of  $\text{Li}^+$  and  $\text{Na}^+$  ions is similar, with  $\text{Na}^+$  ions diffusing slightly faster than  $\text{Li}^+$  ions. This is due to the larger size of  $\text{Na}^+$ , which allows it to be less strongly paired to TFSI than  $\text{Li}^+$ , and thus to exchange its counterions more easily. The influence of metal cations on conductivity is not direct, but rather indirect. Decreasing their correlations with their counterions should lead to an higher conductivity by increasing degrees of freedom of EMIM and TFSI. In order to further investigate charge correlations and related conductivity, it would be necessary to increase the number of trajectories.

Moreover, the soft character and larger radius of  $\text{Na}^+$  ions leads to a higher mobility, especially at low concentration when there are more "free" TFSI. On the other hand, Zn, with its two charges and small size form a strong and stable dimer with TFSI.

In the future design of ionic liquids with high conductivity, soft ions should be preferred. This is because soft ions can more easily form and break connections, leading to higher conductivity.

For applications in energy storage, the design of the IL could be such that the metal cation is less tightly bound to TFSI than EMIM. This points towards a strategy of confinement for reducing metal ion correlations, which could open roads for the development of high-performance ILs for all solid-like energy storage devices. The less tightly paired the metal cation is with TFSI, the more freely it can move, potentially leading to higher conductivity.

## Author Contributions

JLB conceived the study. SKV performed MD simulations, TR performed calibrating MD simulations. YC supervised the simulations. SKV and YC analyzed the results. SKV, YC, CE and JLB contributed the overall interpretation of the results. The manuscript was written by SKV, YC, CE and edited by YC, CE and JLB.

## Conflicts of interest

There are no conflicts to declare.

## Acknowledgements

We thank the GLiCID regional computing mesocentre, supported by Pays de la Loire, for computational support.

## Notes and references

- 1 M. Armand, F. Endres, D. R. MacFarlane, H. Ohno and B. Scrosati, *Nature Materials*, 2009, **8**, 621–629.
- 2 M. Galiński, A. Lewandowski and I. Stępnik, *Electrochimica Acta*, 2006, **51**, 5567–5580.
- 3 M. Smiglak, J. M. Pringle, X. Lu, L. Han, S. Zhang, H. Gao, D. R. MacFarlane and R. D. Rogers, *Chem. Commun.*, 2014, **50**, 9228–9250.
- 4 D. R. MacFarlane, N. Tachikawa, M. Forsyth, J. M. Pringle, P. C. Howlett, G. D. Elliott, J. H. Davis, M. Watanabe, P. Simon and C. A. Angell, *Energy & Environmental Science*, 2013, **7**, 232–250.
- 5 M. Watanabe, M. L. Thomas, S. Zhang, K. Ueno, T. Yasuda and K. Dokko, *Chemical Reviews*, 2017, **117**, 7190–7239.
- 6 G.-T. Kim, S. Passerini, M. Carewska and G. Appetecchi, *Membranes*, 2018, **8**, 41.
- 7 D. T. Rogstad, M.-A. Einarsrud and A. M. Svensson, *Journal of The Electrochemical Society*, 2022, **169**, 110531.
- 8 H. Che, S. Chen, Y. Xie, H. Wang, K. Amine, X.-Z. Liao and Z.-F. Ma, *Energy & Environmental Science*, 2017, **10**, 1075–1101.
- 9 H. Sun, G. Zhu, X. Xu, M. Liao, Y.-Y. Li, M. Angell, M. Gu, Y. Zhu, W. H. Hung, J. Li, Y. Kuang, Y. Meng, M.-C. Lin, H. Peng and H. Dai, *Nature Communications*, 2019, **10**, 3302.
- 10 Y. Zhang, Z. Chen, H. Qiu, W. Yang, Z. Zhao, J. Zhao and G. Cui, *NPG Asia Materials*, 2020, **12**, 4.
- 11 J. Serra Moreno, G. Maresca, S. Panero, B. Scrosati and G. Appetecchi, *Electrochemistry Communications*, 2014, **43**, 1–4.
- 12 M. Kar, B. Winther-Jensen, M. Forsyth and D. R. MacFarlane, *Physical Chemistry Chemical Physics*, 2013, **15**, 7191.
- 13 Q. Huang, T. C. Lourenço, L. T. Costa, Y. Zhang, E. J. Maginn and B. Gurkan, *The Journal of Physical Chemistry B*, 2019, **123**, 516–527.
- 14 J. B. Haskins, J. J. Wu and J. W. Lawson, *The Journal of Physical Chemistry C*, 2016, **120**, 11993–12011.
- 15 M. Gouverneur, F. Schmidt and M. Schönhoff, *Physical Chemistry Chemical Physics*, 2018, **20**, 7470–7478.
- 16 D. Monti, E. Jónsson, M. R. Palacín and P. Johansson, *Journal of Power Sources*, 2014, **245**, 630–636.
- 17 J. M. Vicent-Luna, E. Azaceta, S. Hamad, J. M. Ortiz-Roldán, R. Tena-Zaera, S. Calero and J. A. Anta, *ChemPhysChem*, 2018, **19**, 1665–1673.
- 18 H.-B. Han, S.-S. Zhou, D.-J. Zhang, S.-W. Feng, L.-F. Li, K. Liu, W.-F. Feng, J. Nie, H. Li, X.-J. Huang, M. Armand and Z.-B. Zhou, *Journal of Power Sources*, 2011, **196**, 3623–3632.
- 19 A. Martinelli, A. Matic, P. Jacobsson, L. Börjesson, A. Fericola and B. Scrosati, *The Journal of Physical Chemistry B*, 2009, **113**, 11247–11251.
- 20 P. Kubisiak, P. Wróbel and A. Eilmes, *The Journal of Physical Chemistry B*, 2020, **124**, 413–421.
- 21 O. Borodin, G. A. Giffin, A. Moretti, J. B. Haskins, J. W. Lawson, W. A. Henderson and S. Passerini, *The Journal of Physical Chemistry C*, 2018, **122**, 20108–20121.
- 22 A. Brandt, S. Pohlmann, A. Varzi, A. Balducci and S. Passerini, *MRS Bulletin*, 2013, **38**, 554–559.
- 23 T. Liu, R. Vilar, S. Eugénio, J. Grondin and Y. Danten, *Journal of Applied Electrochemistry*, 2015, **45**, 87–93.
- 24 C. Lethien, J. L. Bideau and T. Brousse, *Energy & Environmental Science*, 2019, **12**, 96–115.
- 25 A. P. Thompson, H. M. Aktulga, R. Berger, D. S. Bolintineanu, W. M. Brown, P. S. Crozier, P. J. In 't Veld, A. Kohlmeyer, S. G. Moore, T. D. Nguyen, R. Shan, M. J. Stevens, J. Tranchida, C. Trott and S. J. Plimpton, *Computer Physics Communications*, 2022, **271**, 108171.
- 26 *fftool*, Padua Group, <https://github.com/paduagroup/fftool>.
- 27 L. Martínez, R. Andrade, E. G. Birgin and J. M. Martínez, *Journal of Computational Chemistry*, 2009, **30**, 2157–2164.
- 28 M. Brehm, M. Thomas, S. Gehrke and B. Kirchner, *The Journal of Chemical Physics*, 2020, **152**, 164105.
- 29 N. Michaud-Agrawal, E. J. Denning, T. B. Woolf and O. Beckstein, *Journal of Computational Chemistry*, 2011, **32**, 2319–2327.
- 30 R. J. Gowers, M. Linke, J. Barnoud, T. J. E. Reddy, M. N. Melo, S. L. Seyler, J. Domański, D. L. Dotson, S. Buchoux, I. M. Kenney and O. Beckstein, *Proceedings of the 15th Python in Science Conference*, 2016, 98–105.
- 31 J. N. Canongia Lopes and A. A. H. Pádua, *Theoretical Chemistry Accounts*, 2012, **131**, 1129.
- 32 R. H. Stote and M. Karplus, *Proteins: Structure, Function, and Bioinformatics*, 1995, **23**, 12–31.
- 33 E. J. Maginn, R. A. Messerly, D. J. Carlson, D. R. Roe and J. R. Elliot, *Living Journal of Computational Molecular Science*, 2020, **2**,.
- 34 P. Kubisiak and A. Eilmes, *The Journal of Physical Chemistry B*, 2017, **121**, 9957–9968.
- 35 P. Wróbel, P. Kubisiak and A. Eilmes, *The Journal of Physical Chemistry C*, 2019, **123**, 14885–14894.
- 36 T. Umecky, Y. Saito and H. Matsumoto, *The Journal of Physical Chemistry B*, 2009, **113**, 8466–8468.
- 37 S. Tsuzuki, W. Shinoda, H. Saito, M. Mikami, H. Tokuda and M. Watanabe, *The Journal of Physical Chemistry B*, 2009, **113**, 10641–10649.
- 38 A. Marie, B. Said, A. Galarneau, T. Stettner, A. Balducci,

M. Bayle, B. Humbert and J. L. Bideau, *Physical Chemistry Chemical Physics*, 2020, **22**, 24051–24058.

39 G. Feng, M. Chen, S. Bi, Z. A. H. Goodwin, E. B. Postnikov, N. Brilliantov, M. Urbakh and A. A. Kornyshev, *Phys. Rev. X*, 2019, **9**, 021024.